



# Separation of overlapping phases for $\text{Se}_{88}\text{Te}_{10}\text{Ag}_2$ glass

D. Hamad<sup>1</sup> · Samar Moustafa<sup>1,2</sup> · M. A. Abdel-Rahim<sup>1</sup> · A. M. Abdelraheem<sup>1</sup>

Received: 14 December 2022 / Accepted: 15 June 2023 / Published online: 17 July 2023  
© The Author(s) 2023

## Abstract

Results of crystallization kinetics for  $\text{Se}_{88}\text{Te}_{10}\text{Ag}_2$  glass using differential scanning calorimetry under non-isothermal condition are described and discussed. The glass has a single glass transition and two crystalline phases that overlap. The Gaussian fit model was used to separate the overlapping crystalline phases. By applying the Matusita et al. approach to analyses the data, it was possible to determine the activation energy ( $E_c$ ) and Avrami exponent ( $n$ ) for the two phases. The average  $E_c$  values for the first and the second phases are 126.16 and 113.99  $\text{kJ mol}^{-1}$ , respectively. It was shown that the activation energy strongly depended on the heating rate. Using the Kissinger–Akahira–Sunose method, the variable activation energies with crystalline fraction are calculated. This variation demonstrates how the transition from the amorphous to the crystalline phase is a complicated process requiring several nucleation and growth mechanisms. It was discussed if the Johnson–Mehl–Avrami model to describe the crystallization for the composition under investigation. The results show SB( $M, N$ ) that model is more appropriate to represent the crystallization process for the examined composition. While the results agree with JMA models at low heating rates. Through the use of scanning electron microscopy and X-ray diffraction, the crystalline phases for the two stages were identified.

**Keywords** Crystallization kinetics · Se–Te–Ag system · Thermal analysis · X-ray diffraction · SEM examination

## Introduction

The use of chalcogenide glasses in a variety of solid-state electronics has considerable attention. There are many applications for chalcogenide glasses, including threshold switching, memory switching, and optical wave guides [1, 2]. The transport mechanism, thermal stability, and optical applicability of the chalcogenide glass are influenced by structural properties. Numerous experimental methods, including electron microscopy, X-ray diffraction, and thermal analysis, have been employed to investigate the structure of chalcogenide glasses [3, 4].

The selection of Se because exhibits a unique property of reversible transformation which makes it very useful in optical memory devices [5]. Pure Se generally has drawbacks due to its brief lifetime and low photosensitivity. Many attempts have been made to improve the Se properties by

alloying it with other elements [6]. In comparison to pure Se, the glassy Se–Te alloys have greater hardness, a higher crystallization temperature, more photosensitive, and fewer ageing effects [4]. Furthermore, xerography and electrographic applications, as well as outstanding laser writer sensitivity. The addition of the third element to Se–Te increases the glass-forming region and gives a new promising properties [7]. On the other hand, the addition of Ag to Se–Te creates compositional and configurational change as compared the binary alloy [8]. The transformation from amorphous to crystalline phase for chalcogenide glasses doping with Ag content has been studied by many workers [8–10] for development of new and gives better phase change recording materials. Mehta et al. [10] have investigated the crystallization process for Se–Te–Ag glasses. These glasses have only endothermic and one exothermic peaks at low concentration of Ag content. However, at higher concentration of Ag, two endothermic and two exothermic peaks have been observed in these glasses. Many researchers [11–13] studying the properties of the Se–Te–Ag chalcogenide glasses such as optical, electrical, and thermal stability. The thermal analysis is very important tools for explaining the crystallization process. For many chalcogenide glasses', the crystallization transformations have been explored using the

✉ D. Hamad  
dalia.abdelaal@aun.edu.eg

<sup>1</sup> Physics Department, Faculty of Science, Assiut University, Assiut 71516, Egypt

<sup>2</sup> Physics Department, College of Science, Taibah University, Medina, Saudi Arabia

Johnson–Mehl–Avrami (JMA) or empirical Sestatak Berggren SB( $M$ ,  $N$ ) models [14]. Typically, the following equation can be used to describe the measured heat flow  $\phi$ :

$$\phi = \Delta HA \exp\left(\frac{-E_C}{RT}\right) f(\alpha) \quad (1)$$

where  $\Delta H$  is the crystallization enthalpy,  $A$  is the pre-exponential factor,  $E_C$  is the apparent activation energy,  $R$  is the universal gas constant, and  $T$  is the temperature. The JMA model describes the function  $f(\alpha)$  as [15]:

$$f(\alpha) = n(1 - \alpha)[- \ln(1 - \alpha)]^{1-1/n} \quad (2)$$

where  $n$  is a Avrami index and  $\alpha$  define the degree of crystallization. Furthermore, the SB( $M$ ,  $N$ ) model can be used to describe the function  $f(\alpha)$  as follows [16]:

$$f(\alpha) = \alpha^M(1 - \alpha)^N \quad (3)$$

The two kinetic parameters  $M$  and  $N$  show, the acceleratory and decaying regions' relative for the transformation process. The value of  $M$  is limited in range ( $0 < M < 1$ ).

The two characteristic functions  $y(\alpha)$  and  $z(\alpha)$  for non-isothermal condition given by Malek to test the applicability of JMA model's [17]:

$$y(\alpha) = \phi \exp(E_C/RT) \quad (4)$$

$$z(\alpha) = \phi T^2 \quad (5)$$

Within the (0, 1) range, the functions  $y(\alpha)$  and  $z(\alpha)$  are normalized. The two  $y(\alpha)$  and  $z(\alpha)$  functions has a maximum value when  $\alpha$  equal to  $\alpha_M$  and  $\alpha_p^\infty$ , respectively. The value of  $\alpha_M$  is typically less than  $\alpha_p^\infty$ . For the JMA model, the latter is a constant ( $\alpha_p^\infty = 0,632$ ). The  $\alpha_M$  is a fingerprint for JMA model's [18]. Malek et al. provide specific information regarding  $y(\alpha)$ ,  $z(\alpha)$ , and their maxima of  $\alpha_M$  and  $\alpha_p^\infty$  [18].

In this work, concerned to study the structure of  $\text{Se}_{88}\text{Te}_{10}\text{Ag}_2$  glass using different techniques such as XRD, SEM, and DSC. The JMA models and SB( $M$ ,  $N$ ) empirical equation's used for deduced the kinetic parameters. Finally, X-ray diffraction and scanning electron microscopy (SEM) analysis were used to identify the crystal phases that corresponded to crystallization events.

## Experimental technique

The amorphous materials for Se–Te–Ag chalcogenide glass are prepared by the melt quenching technique, which described in detailed elsewhere [19]. In this technique, glasses were weighted according to their percentages using high purity (99.99%) Se, Te, and Ag (from 5 N, sigma-Aldrich).

Glasses were sealed in a silica ampules under a vacuum of  $10^{-5}$  Torr. The ampules were heated in a rotating furnace at 1273 K for 24 h. continuous stirring of the melt was carried out to ensure good homogeneity. The ampules were then quenched in ice–water mixture. The DSC analysis for as-prepared powdered under non-isothermal condition using a PerkinElmer DSC-2. The DSC curves take place from room temperature to melting temperature at different heating rates ranging from 2.5 to 20 K min<sup>-1</sup>. The instrument was calibrated using In, Sn and Pb standards of known heat capacity and melting points. The temperature accuracy of the instrument is  $\pm 0.1$  K with heat flow accuracy of  $\pm 0.01$  mw transition. The microprocessor of the thermal analyzer was used to determine the values of the glass transition temperature ( $T_g$ ), the onset temperature ( $T_c$ ), the peak of crystallization temperature ( $T_p$ ), and the melting temperature ( $T_m$ ) with an average standard error of  $\pm 1$  K.

The samples were coated with gold before SEM examination to avoid the charging effect. Scanning electron microscopy (SEM) apparatus (Joel, JSM-T200 type, Japan) was used to examine the surface morphology of the annealed  $\text{Se}_{88}\text{Te}_{10}\text{Ag}_2$  samples at different temperature for 1 h. The elements in the composition  $\text{Se}_{88}\text{Te}_{10}\text{Ag}_2$  were determined by using energy dispersive X-ray analysis (EDX) spectroscopy. Additionally, the crystalline phase and amorphous nature of the as-prepared and annealed samples were analyzed using the X-ray diffraction technique (XRD) using a Philips Diffractometer (type 1710, Netherland). The XRD scans recorded in diffraction angle  $2\theta$  in range ( $10^\circ \leq 2\theta \leq 80^\circ$ ) with scanning speed of 3.6° min<sup>-1</sup> and Cu K $\alpha$  radiation of wavelength  $\lambda$  equals 1.5406 Å.

## Results and discussion

### Thermal and structural characterization

Typical DSC curves of the crystallization process were recorded at different heating rates ranging from 2.5 to 20 K min<sup>-1</sup> for  $\text{Se}_{88}\text{Te}_{10}\text{Ag}_2$  composition are shown in Fig. 1. The DSC curve shows first strong exothermic peak partially overlapped by weak exothermic peak. The overlap peaks can also indicate that the nucleation and crystal growth occur simultaneously. If the overlap is negligible this can be ignored while when the degree of overlap is large, then, it is necessary to resolve the complex peak. The two overlapping peaks resolved by Gaussian model. Figure 2 shows the separation of the two overlapping crystallization peaks at heating rate 20 K min<sup>-1</sup>. Also, the endothermic peak in DSC scans gives the glass transition from amorphous phase to the super-cooled liquid state. Numerical values of  $T_g$ ,  $T_{c1}$ ,  $T_{c2}$ ,  $T_{p1}$ , and  $T_{p2}$  with different heating rate are listed in Table 1. As shown from Table 1, the temperatures  $T_g$ ,  $T_{c1}$ ,  $T_{c2}$ ,  $T_{p1}$ ,

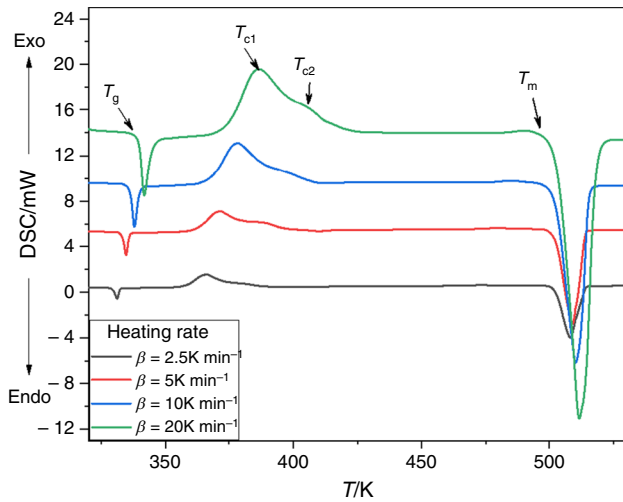


Fig. 1 Typical DSC curves for Se<sub>88</sub>Te<sub>10</sub>Ag<sub>2</sub> glass at different heating rates

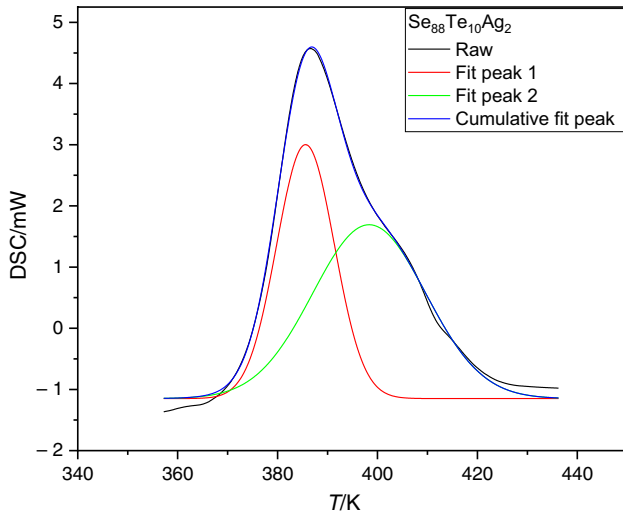


Fig. 2 Separation of the two overlapped peaks for Se<sub>88</sub>Te<sub>10</sub>Ag<sub>2</sub> glass

and  $T_{p2}$  for the studied composition increased with increasing the heating rates. The relaxation dynamics during the glass transition period may be responsible for the increase in  $T_g$  with heating rate ( $\beta$ ). As the heating rate  $\beta$  increased, the time decreased; hence, the  $T_g$  increased [20]. Also, when the heating rates are increased, the intensities of all DSC peaks for the first and second peaks increased as shown in Fig. 3. Additionally, when the heating rates increased, the two peaks shifted to higher temperatures, indicating the crystallization process occurs as a result of the thermal activation.

**The glass transition region**

The variation  $T_g$  with  $\ln \beta$  found to be linear as shown in Fig. 4 which satisfying Lasocka formula [21] as follows:

$$T_g = A + B \ln \beta \tag{6}$$

where  $A$  and  $B$  are constant for the studying glass. The deduced values for  $A$  and  $B$  are 325 and 4.9, respectively. The empirical relationship for Se<sub>88</sub>Te<sub>10</sub>Ag<sub>2</sub> can be written as  $T_g = 324.95 + 4.89 \ln \beta$

The activation energy  $E_g$  for glass transition determined by using Kissinger’s formula [22]:

$$\ln \left( \beta / T_g^2 \right) = \frac{-E_g}{RT_g} + \text{constant} \tag{7}$$

Figure 5 shows  $\ln \left( \beta / T_g^2 \right)$  versus  $1000/T_g$  for the studying composition. The deduced value of  $E_g$  is 184.22 kJ mol<sup>-1</sup>. This value agrees with values obtained by other works [1, 2, 4]. Furthermore, the difference between  $T_C$  and  $T_g$  gives the kinetic resistance to crystallization. The glass samples with lower ( $T_C - T_g$ ) values are predicted to have lower thermal stability, higher electrical conductivity, and lower crystallization resistance [3]. Hurby [23] provides another parameter named the glass forming tendency (GFA):

**Table 1** Glass transition, the crystallization onset and the activation energy ( $E_c$ ) for the Se<sub>88</sub>Te<sub>10</sub>Ag<sub>2</sub> glass at different heating rates

Heating rate ( $\beta$ )/K min <sup>-1</sup>	$T_g$	$T_{c1}$	$T_{p1}$	$H_r$	$E_c$
<i>Peak (1)</i>					
2.5	329.3	356.3	365.5	000.19	149.6
5	333.1	360.8	370.7	000.20	138.6
10	336.1	364.1	377.6	000.21	113.2
20	339.6	369.5	385.6	000.24	103.3
<i>Peak (2)</i>					
	$T_g$	$T_{c2}$	$T_{p2}$	$H_r$	$E_c$
2.5	329.3	359.6	375.5	000.22	134.6
5	333.1	365.2	383.6	000.24	118.5
10	336.1	368.7	390.0	000.25	111.7
20	339.6	368.7	398.3	000.23	090.9

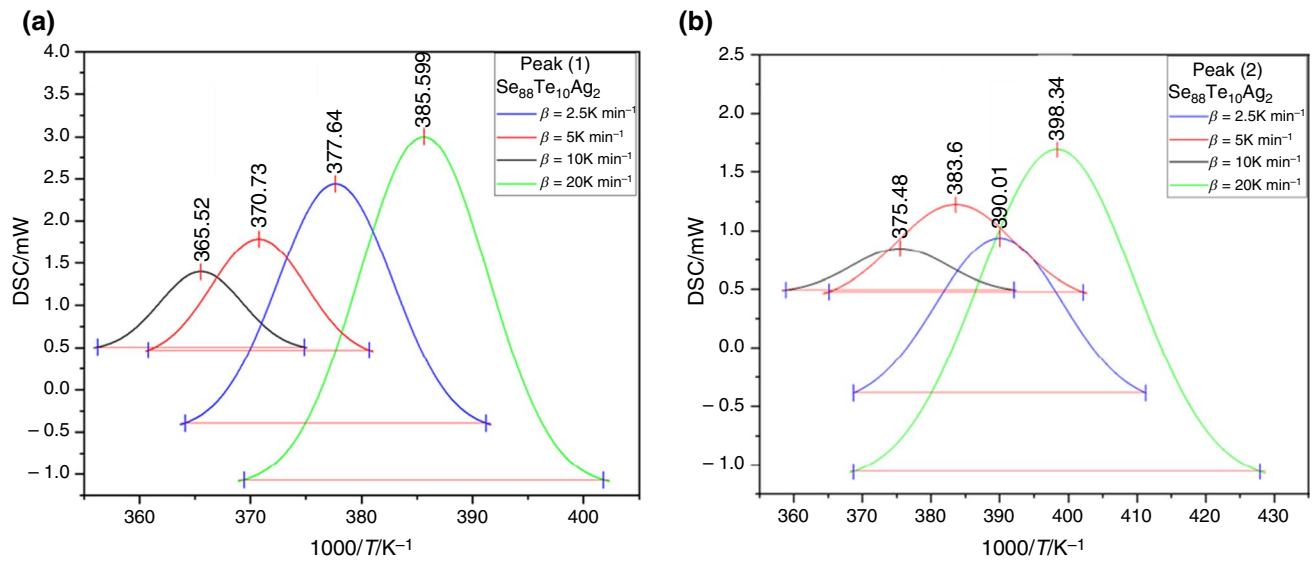


**Fig. 3** DSC scan for as-prepared  $\text{Se}_{88}\text{Te}_{10}\text{Ag}_2$  glass at different heating rates for the two exothermic peaks

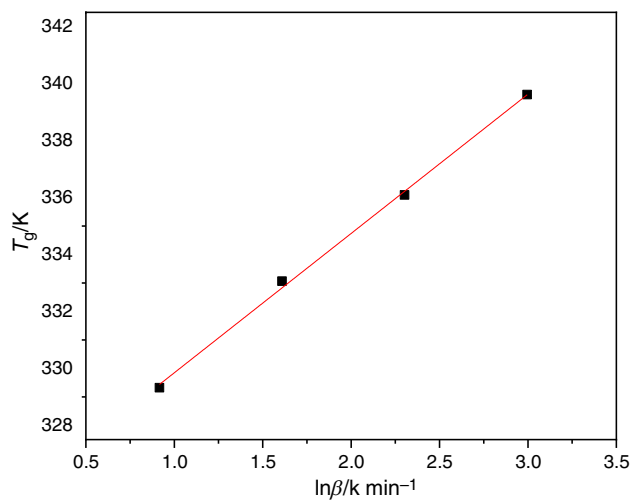


**Fig. 4** Variation of  $T_g$  versus  $\ln \beta$  for the composition  $\text{Se}_{88}\text{Te}_{10}\text{Ag}_2$  glass

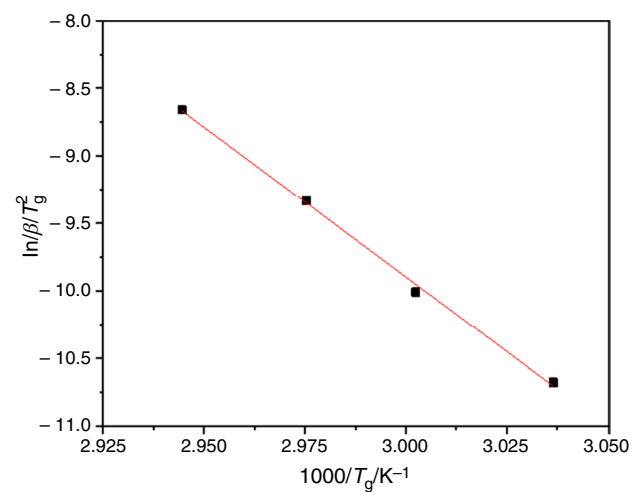


**Fig. 5** Variation of  $\ln(\beta/T_g^2)$  versus  $1000/T_g$  for the composition  $\text{Se}_{88}\text{Te}_{10}\text{Ag}_2$  glass

$$H_r = \frac{T_C - T_g}{T_m - T_C} \quad (8)$$

The probability of finding glass is determined by the parameter  $H_r$ , which rises as  $T_m - T_C$  falls and  $T_C - T_g$  rises. According to  $H_r$  number, it is difficult to prepare glass at  $H_r \leq 0.1$  but good glass is obtained at  $H_r \geq 0.4$  [23]. The calculated values of  $H_r$  for the investigated composition at various heating rates are listed in Table 1. The average  $H_r$  values provide satisfactory glass for the investigated composition.

### Crystallization mechanism

The Matusita method was used to compute the crystallization kinetic parameters based on the JMA model; specifically, the crystallization activation energy  $E_c$  and the Avrami exponent ( $n$ ) can be deduced using the following equation [24]:

$$\ln[-\ln(1-\alpha)] = -n \ln \beta - 1.052 \frac{mE_c}{RT} + \text{const.} \quad (9)$$

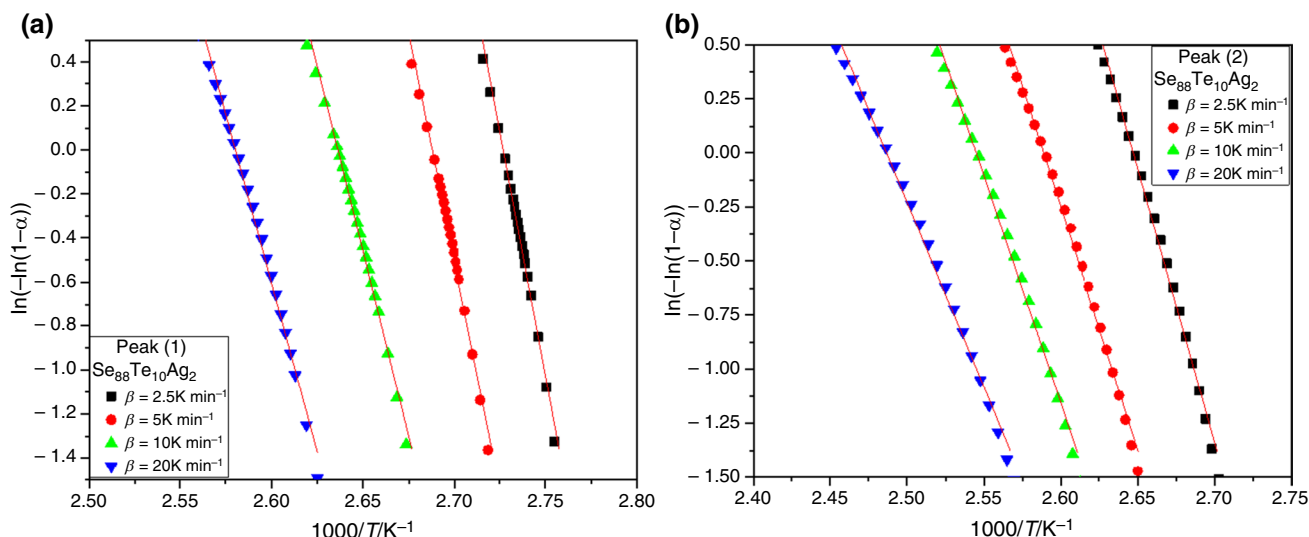


**Fig. 6** a and b The plots of  $\ln[-\ln(1-\alpha)]$  versus  $1000/T$  at different heating rates for  $\text{Se}_{88}\text{Te}_{10}\text{Ag}_2$  glass

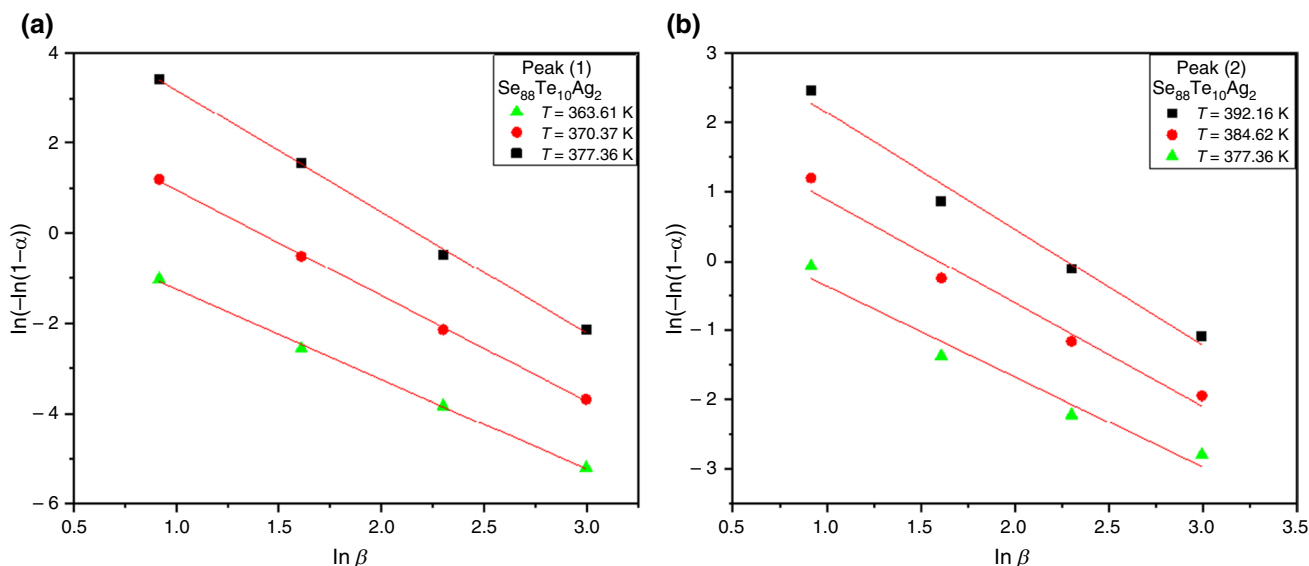


**Fig. 7** a and b The plots of  $\ln[-\ln(1-\alpha)]$  versus  $\ln \beta$  at different three temperatures for  $\text{Se}_{88}\text{Te}_{10}\text{Ag}_2$  glass

where  $n$  and  $m$  are integer which depends on the dimensionality of the crystal growth. For quenching glass no nuclei then  $n = m + 1$ ; however, if nuclei formed after any earlier heat treatment before thermal analysis, then,  $n = m$ . In this study, we consider  $n = m$  because the sample heated to a temperature below the glass transition ( $T_g$ ) before each experimental run. The  $mE_c$  values were calculated from the graphs of  $\ln(-\ln(1-\alpha))$  versus  $1000/T$  for the two peaks illustrated in Fig. 6a and b at various heating rates. A break in the linearity observed at higher temperatures. This breaks in the linearity due to the final stage of crystallization's nucleation

sites becoming saturated [1, 24]. Additionally, the following equation can be used to derive the Avrami exponent ( $n$ ):

$$\left[ \frac{d \ln(-\ln(1-\alpha))}{d \ln \beta} \right]_T = -n \tag{10}$$

The value of  $n$  for the two phases can be obtained by plotting  $\ln(-\ln(1-\alpha))$  against  $\ln \beta$  at different temperatures as shown in Fig. 7a and b for the studied composition. From this figure, it is observed that  $n$  is temperature independent. The average deduced values of  $n$  are  $2.35 \pm 0.2$  and

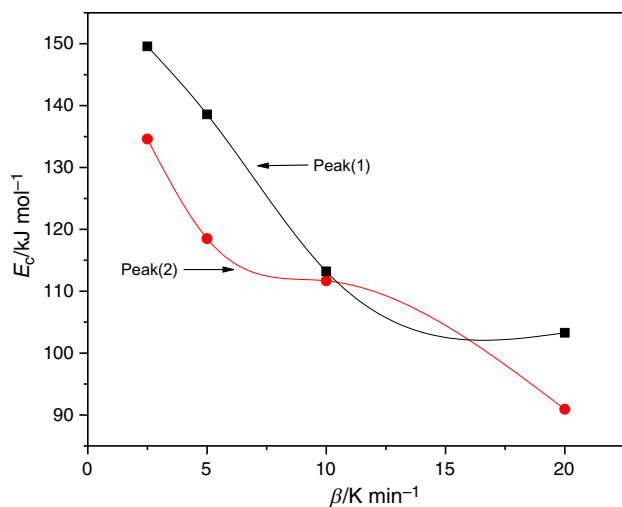


**Fig. 8** Variation of  $E_c$  versus  $\beta$  for the compositions  $\text{Se}_{88}\text{Te}_{10}\text{Ag}_2$  chalcogenide glass

$1.49 \pm 0.25$  for the first and second peaks, respectively. The deduced  $n$  values are not integers. This indicates that the crystallization mechanism is a composite of many mechanisms. The effective activation energies  $E_c$  for  $\text{Se}_{88}\text{Te}_{10}\text{Ag}_2$  were calculated from the average  $n$  and  $mE_c$  values. Figure 8 illustrates the change of  $E_c$  values versus  $\beta$  for the two phases. The results demonstrate a dramatic drop in  $E_c$  as the heating rates increased. The average values of  $E_c$  for the first and second phases are  $126.16 \text{ kJ mol}^{-1}$  and  $113.92 \text{ kJ mol}^{-1}$ , respectively. It is observed that  $E_{c2} < E_{c1}$  indicates that the energy barrier of the first phase is higher than that of the second phase implying that the second stage of crystallization is easier to be occurred. Additionally, decreasing the activation energy  $E_{c2}$  of the second peak means that the nucleation

takes place during the first phase of crystallization process [25]. These results agree with other works [25, 26].

The Avrami index  $n$  and the activation energy  $E_c$  must be constant during the transformation process, according to the JMA model [1]. However, several researchers have demonstrated that  $n$  and  $E_c$  values, in both isothermal and non-isothermal approaches are not necessary constant but changed during the transformation process [19, 26]. The variation of  $n$  and  $E_c$  values with  $\alpha$  throughout the transformation process is defined as the change of nucleation and growth process [27].

### Evaluation of the activation energy using iso-conversion models

The change in the activation energy  $E_c$  with the crystallization fraction ( $\alpha$ ) can be defined by the local activation energy  $E(\alpha)$ . The local activation energy  $E_c(\alpha)$  can be deduced for the two phases by using different iso-conversion methods. One of these methods named Kissinger Akahira–Sunose (KAS) [28]:

$$\ln\left(\frac{\beta}{T_\alpha^2}\right) = \text{const} - E_\alpha/RT_\alpha \quad (11)$$

The  $E_c(\alpha)$  values for the first and second stages deduced from the plots of  $\ln(\beta/T_\alpha^2)$  versus  $1000/T_\alpha$  at various  $\alpha$  ( $0.1 \leq \alpha \leq 0.9$ ) as shown in Fig. 9a and b. As illustrated in Fig. 10, it is observed that the  $E_c$  values are not constant for the two crystallization stages and decrease with increasing  $\alpha$ . The average  $E_c(\alpha)$  values for the first and second phases are  $114.71 \text{ kJ mol}^{-1}$  and  $109.9 \text{ kJ mol}^{-1}$ , respectively. These average values are lower than the apparent activation energies obtained by Matusita model for the two phases. The

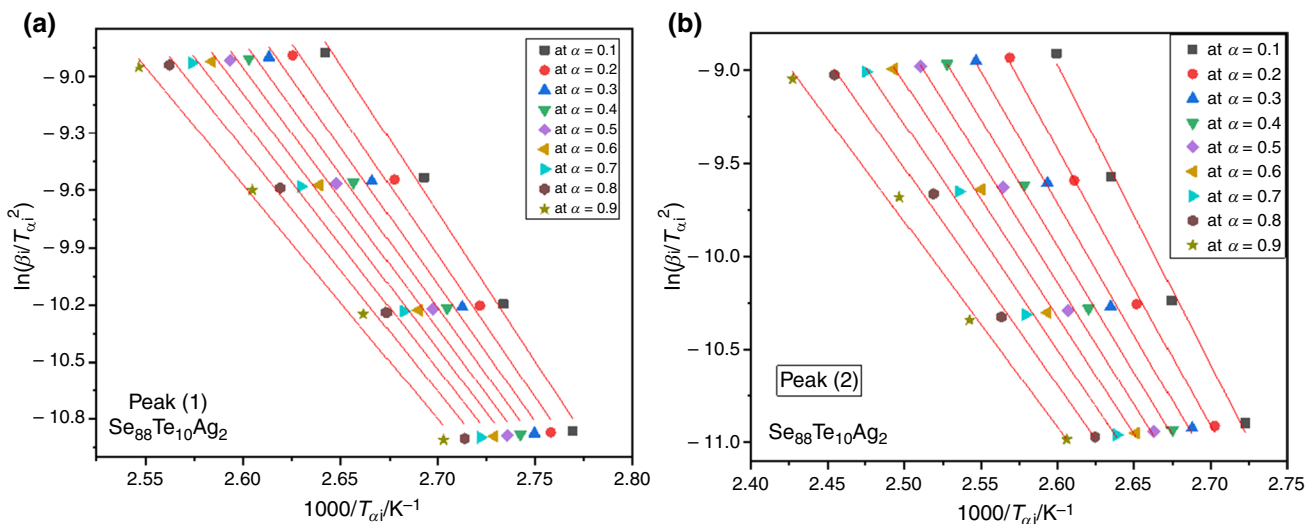


**Fig. 9** a and b The plots of  $\ln(\beta/T_\alpha^2)$  versus  $1000/T_\alpha$  at different heating rates for  $\text{Se}_{88}\text{Te}_{10}\text{Ag}_2$  glass



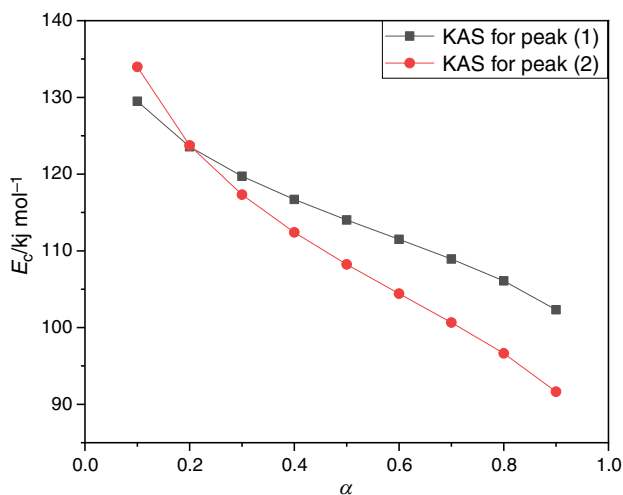


**Fig. 10** Effective activation energy as a function of  $\alpha$  for  $\text{Se}_{88}\text{Te}_{10}\text{Ag}_2$  glass

change in  $E_c(\alpha)$  values with the crystallize volume  $\alpha$  means the crystallization process exhibits nucleation and growth processes [29] has activation energy  $E_n$  and  $E_g$ , respectively.

In general, the local activation energy  $E_c(\alpha)$  can be expressed as follows:

$$E_c(\alpha) = aE_n + bE_g \quad (I \geq 0, u \geq 0) \tag{12}$$

where  $I$  and  $u$  are the nucleation rate and growth velocity, respectively,  $a$  and  $b$  are two variables which are both less than or equal to one and more than or equal to 0. The early stages of crystallization are dominated by nucleation, with  $u = 0, a = 1, b = 0$  and activation energies as  $E_c(0) = E_n = 135 \text{ kJ mol}^{-1}$  for the first stage and  $138 \text{ kJ mol}^{-1}$  for the second stage. As crystallization

progresses, nucleation and grain growth influence the crystallization kinetics, where  $a$  decrease and  $b$  rise as crystallization progresses. Therefore, as the crystalline percentage increases, the values  $E_c(\alpha)$  decreases with increasing  $\alpha(0 < \alpha < 1)$ . When  $I = 0$ , and  $a = 0, b = 1$  and the activation energies  $E_c(1) = E_g = 103 \text{ kJ mol}^{-1}$  and  $88 \text{ kJ mol}^{-1}$  for the first and second stages, respectively. The crystallization is dominated by grain growth in the final stage. In general, the variation of  $E_c(\alpha)$  values for the two crystallization stages indicates that the crystallization process is complicated [29, 30].

### Transformation model

The second step for the kinetic analysis which gives the kinetic model to describe the crystallization process for  $\text{Se}_{88}\text{Te}_{10}\text{Ag}_2$ . According to Malek model [15], the reliable test for the validity of JMA model to describe the crystallization process based on the maximum value of  $Z(\alpha)$  is  $\alpha_p^\infty$ . The experimental DSC could be represented by the JMA model if the values of  $\alpha_p^\infty$  in the range of 0.61–0.65. On the other hand, the JMA model not applicable if  $\alpha_p^\infty$  has lower values. This test is applicable for our composition. According to Eqs. (4) and (5), we deduced the changes of  $y(\alpha)$  and  $z(\alpha)$  functions.

The average values of  $E_c(\alpha)$  deduced by Kissinger–Aka-hira–Sunose (KAS) model were used to calculate  $y(\alpha)$  function for the two crystallization phases. Figure 11a and b shows the deducing  $y(\alpha)$  and  $z(\alpha)$  functions as a function of  $\alpha$  for the two crystallization events at different heating rates. The maximum value of  $\alpha_p^\infty$  for  $z(\alpha)$  function around 0.5 for the first phase at all heating rates as shown in Fig. 12. a On the other hand, the maximum value of  $\alpha_p^\infty$  for the second stage changed with the heating rates as shown

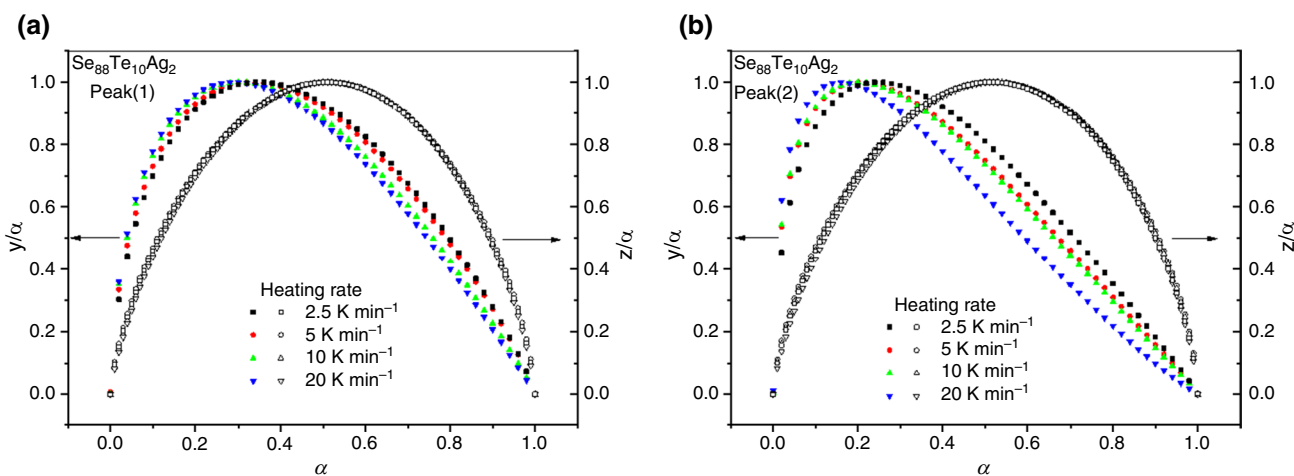


**Fig. 11** a and b Normalized  $y(\alpha)$  and  $z(\alpha)$  functions at the different heating rates for  $\text{Se}_{88}\text{Te}_{10}\text{Ag}_2$  glass

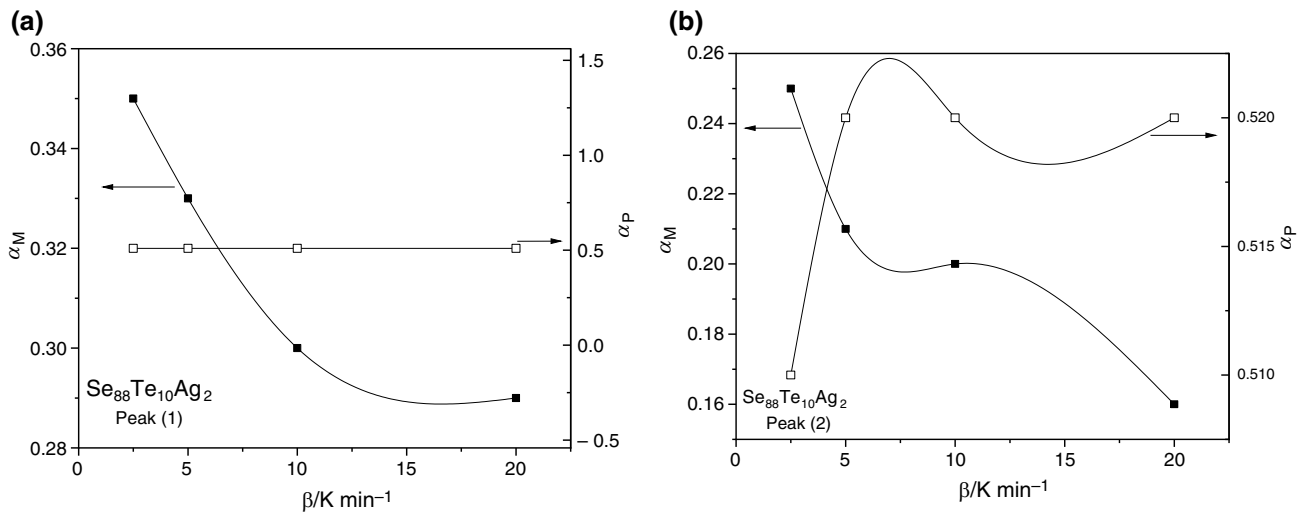


**Fig. 12** a and b Variation of  $\alpha_M$  and  $\alpha_p$  versus  $\beta$  for the compositions  $\text{Se}_{88}\text{Te}_{10}\text{Ag}_2$  glass

in Fig. 12b. For the second phase, the  $\alpha_p^\infty$  value increased from 0.17 to 0.52 when heating rate increased from 2.5 to 20  $\text{K min}^{-1}$ . In general, the value of  $\alpha_p^\infty$  is significantly smaller than the fingerprint of the JMA model (0.63–0.65) for the two crystallization stages. Furthermore, for the two phases, the values of  $\alpha_M$  decreasing with increasing the heating rates as shown in Fig. 12 a and b. This gives a more complicated crystallization process [29] for the studied composition. Therefore, we conclude that the JMA model is not appropriate for studying the crystallization kinetics for  $\text{Se}_{88}\text{Te}_{10}\text{Ag}_2$  glass. In this case, Sestuck–Berggren SB( $M, N$ ) model should be applied for analyzed the crystallization kinetics for the studied composition. The ratio between  $M$  and  $N$  is expressed through the following equation [31]:

$$\frac{M}{N} = \frac{\alpha_M}{1 - \alpha_M} \quad (13)$$

The average values of  $E_c(\alpha)$  deduced by KAS method are used to find  $\alpha_M$ . Also, the  $N$  value are deduced using the following equation [31]:

$$\ln [\phi \exp (E_c/RT)] = \ln (\Delta HA) + N \ln [\alpha^{M/N}(1 - \alpha)] \quad (14)$$

This relation is valid in the range  $0.2 \leq \alpha \leq 0.8$  [27]. The  $N$  values were deduced from the slope of the plots of  $\ln [\phi e^{E_c/RT}]$  versus  $\ln [\alpha^{M/N}(1 - \alpha)]$  with different heating rates for the two phases, as shown in Fig. 13. Using Eq. (13) and the deduced  $N$  value, the average  $M$  can be determined. Also, the intersections of these plots are used to calculate the values of the pre-exponential factor ( $A$ ). Furthermore, the Avrami index  $n$  and  $A$  value deduced using the following formula [31]:

$$\ln [\phi \exp (E_c/RT)] = \ln (\Delta HA) + \ln \{n(1 - \alpha)[- \ln (1 - \alpha)]^{1-1/n}\} \quad (15)$$

Figure 14a and b shows the plots of  $\ln [\phi \exp (E_c/RT)]$  versus  $\ln \{n(1 - \alpha)[- \ln (1 - \alpha)]^{1-1/n}\}$  for the two events of  $\text{Se}_{88}\text{Te}_{10}\text{Ag}_2$  glass. Table 2 summarizes the parameters  $M$ ,  $N$ ,  $A$ ,  $\Delta H$ , and  $n$  for the two phases.

Based on the JMA and SB models, the theoretical DSC curves deduced using Eqs. (2) and (3) as shown in Fig. 15a–d for the studied composition. It is shown that DSC curves deduced by the JMA model agree with the experimental data at the low heating rates for the two crystallization stages. While at high heating rates, the discrepancy becomes large. On the other hand, the experimental DSC data for the two phases are agreement with the DSC curves deduced by using SB( $M, N$ ) model for the studied composition. The deviations of the experimental DSC data from the calculated curve using JMA model at high heating rates may be related to the fact that some approximations used for deriving Eq. (2). Then, the JMA model are not applicable at high heating rate for analysis the crystallization process of  $\text{Se}_{88}\text{Te}_{10}\text{Ag}_2$  glass. Equation (2) can be applied for the studying composition if we consider the entire nucleation process must take place during the early stages of the crystallization kinetic and become negligible afterwards. The temperature is the only factor that influences on the crystallization rate, and the thermal history can be ignored [1, 31]. Generally, at low heating rates, the nuclei have more time to form before the growth process starts. Additionally, the entire nucleation occurs at the initial stages of crystallization. Thus, the JMA model is valid at low heating rates as a result of formation of the grains in nanoscale for the investigated glass. The nuclei expand very slowly after the nucleation process. The



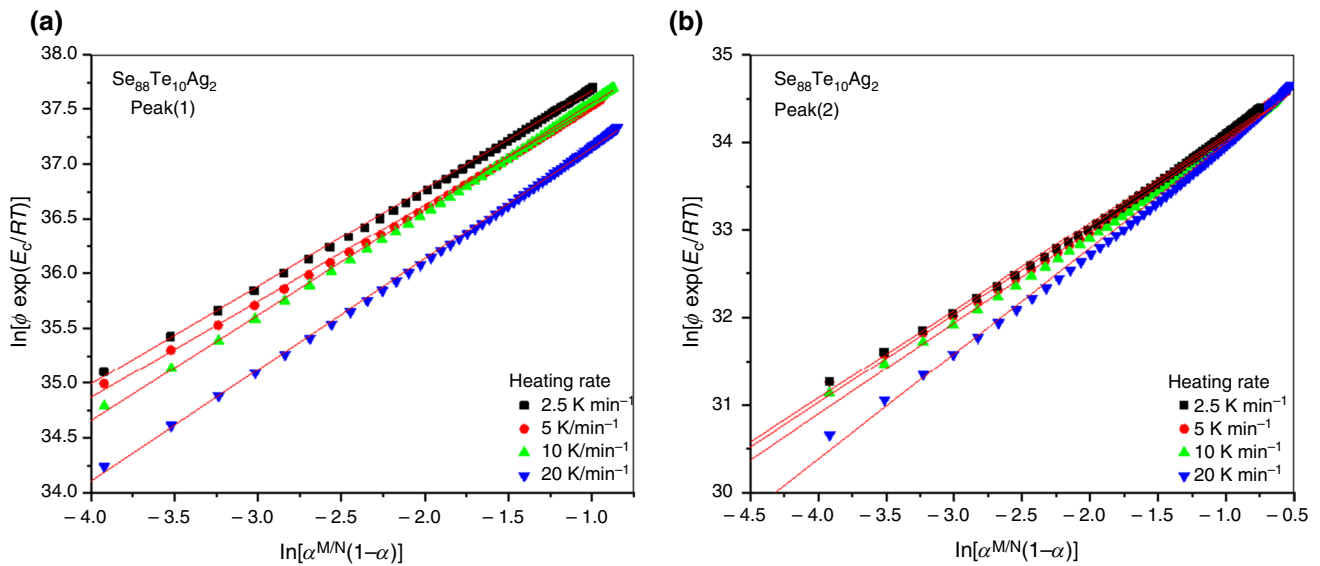


**Fig. 13** a and b The plots of  $\ln[\phi \exp(E_c/RT)]$  versus  $\ln[\alpha^{M/N}(1-\alpha)]$  at different heating rates for  $\text{Se}_{88}\text{Te}_{10}\text{Ag}_2$  glass.

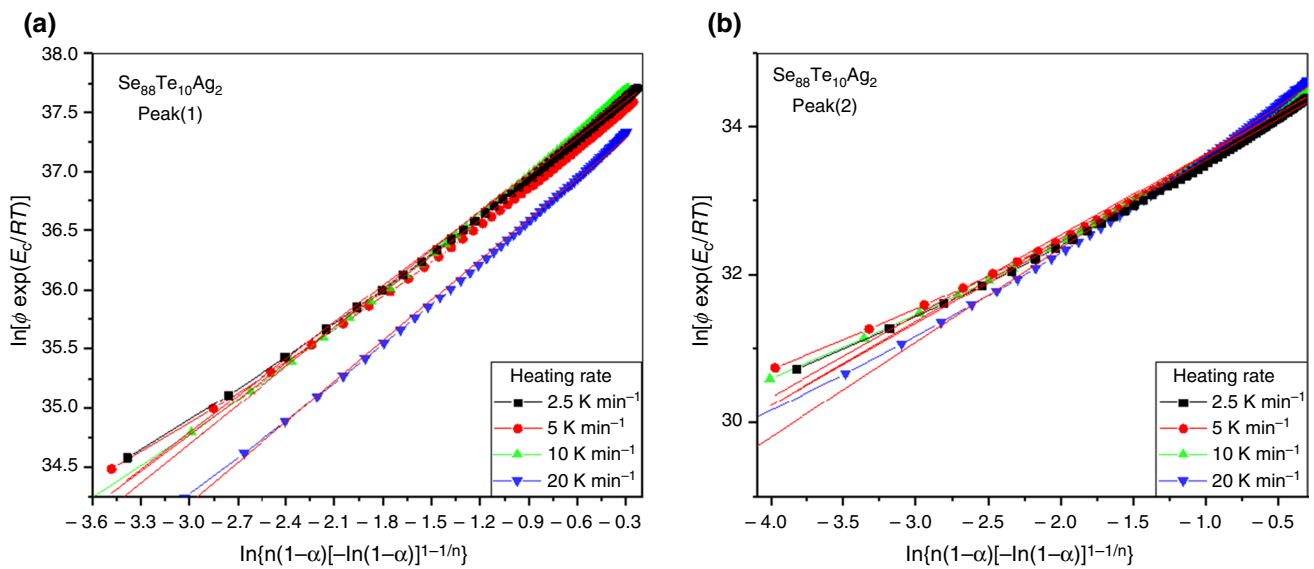


**Fig. 14** a and b The plots of  $\ln[\phi \exp(E_c/RT)]$  versus  $\ln\{n(1-\alpha)[- \ln(1-\alpha)]^{1-1/n}\}$  at different heating rates for  $\text{Se}_{88}\text{Te}_{10}\text{Ag}_2$  glass

temperature quickly raise at high heating rates and according to JMA model the growth process does not take the linear or parabolic growth rate. In general, the JMA model is a special case of the Sestak and Berggan ( $M, N$ ) model. In general, for more complex phases involving both nucleation and growth, the SB( $M, N$ ) model is more suitable for studying the crystallization analysis for our composition.

The transformation from amorphous to crystalline that appeared in DSC scans was studied by SEM examination. Figure 16a–c shows the morphology of the isothermal annealing samples at three different temperatures for 1 h. It

is clear that the crystalline structures have unstable phases with different shapes and size embedded in amorphous matrix are not easily identified for the sample annealed at 350 K. Some of these crystallize phase are collected, and others are isolated. On the other hand, the morphology of the annealed sample at 360 K reveals that the rod like structure imbedded in a metastable phase as shown in Fig. 16b. The stable and unstable crystalline phases represent the first and second overlapping crystalline phases that appeared in DSC curves. Further increasing the annealing temperature near to 370 K, the metastable phases transformed to a stable phase

**Table 2** Crystallization enthalpy,  $\Delta H$ , the parameters of the SB( $M$ ,  $N$ ) and JMA models for  $\text{Se}_{88}\text{Te}_{10}\text{Ag}_2$  glasses at different heating rates

Heating rate ( $\beta$ )/K min <sup>-1</sup>	$\Delta H$ /J g <sup>-1</sup>	SB			JMA	
		$M$	$N$	Ln $A$	$n$	Ln $A$
<i>Peak (1)</i>						
2.5	007.9	000.5	000.9	036.5	001.8	035.80
5	013.2	000.4	000.9	035.8	001.7	035.20
10	035.6	000.4	001.0	034.9	001.6	034.40
20	057.7	000.4	001.0	034.1	001.5	033.6
<i>Peak (2)</i>						
2.5	005.9	000.33	001.0	033.3	001.4	032.9
5	015.1	000.27	001.0	032.4	001.3	032.0
10	028.1	000.26	001.0	031.7	001.3	031.4
20	075.2	000.23	001.2	030.9	001.2	030.6

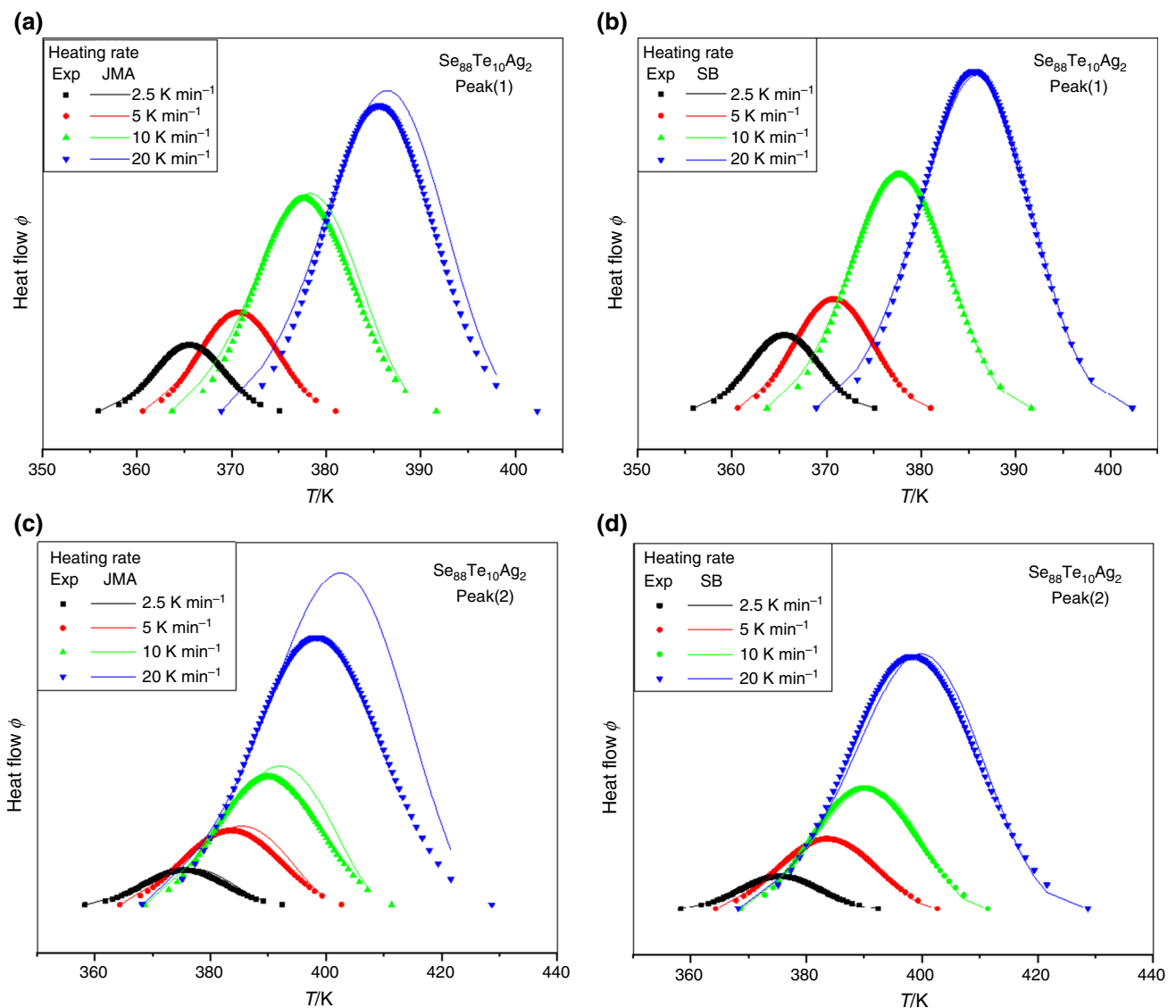
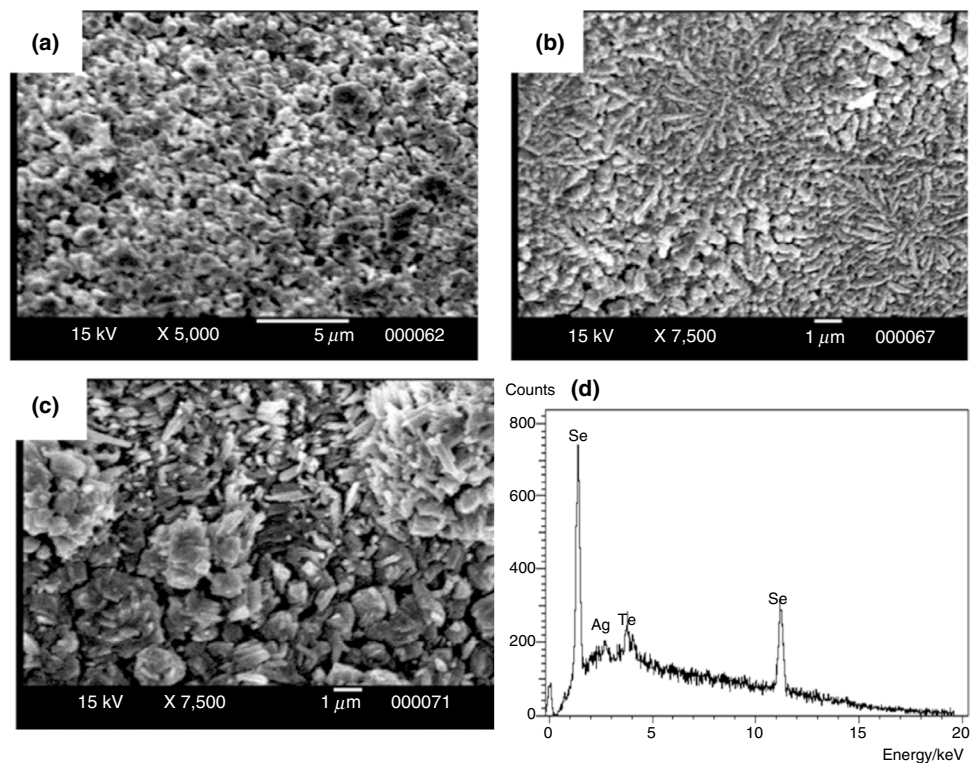


**Fig. 15** a–d Experimental non-isothermal crystallization at different heating rates compared with the calculated data using SB model and JMA using the appropriate activation energy for  $\text{Se}_{88}\text{Te}_{10}\text{Ag}_2$  glass

**Fig. 16** SEM of  $\text{Se}_{88}\text{Te}_{10}\text{Ag}_2$  glass for the isothermal annealing samples at three different temperatures for 1 h. **a** 350 K, **b** 360 K, and **c** 370 K **d** EDX chart for as-prepared of  $\text{Se}_{88}\text{Te}_{10}\text{Ag}_2$



with plate like structure and rod like structure as shown in Fig. 16c. These results are in agreement with first and second overlapping crystalline phases in DSC scans. Energy-dispersive X-ray spectroscopy (EDX) analysis of the as-prepared  $\text{Se}_{88}\text{Te}_{10}\text{Ag}_2$  is shown in Fig. 16d which confirms the presence of the elements Se, Te, and Ag. As shown in this figure, no other impurity peak was observed in the EDX spectrum which indicates high purity of the studied composition. In general, the relative proportions of Se, Te, and Ag for the studied composition are 86.82 at%, 11.17 at%, and 3.01 at%, respectively, which agree nearly with the starting elements.

X-ray diffraction used to identify the crystalline phases that appeared in overlapping phases in DSC scans and SEM examination. Figure 17 shows X-ray diffraction for as-prepared and annealed samples at three different temperatures for 1 h. The X-ray spectra for as-prepared sample do not contain any prominent peak which confirms amorphous nature as show in Fig. 17. On the other hand, the analysis of X-ray diffractions for the annealed samples shows the dominant crystalline phases are Se and AgTe. The AgTe phase was found to crystallize in Orthorhombic structure with a unit cell defined by  $a = 8.900 \text{ \AA}$ ,  $b = 20.070 \text{ \AA}$ , and  $c = 4.620 \text{ \AA}$

according to the ICDS card No. (00-016-0412), while Se phase crystallized in Hexagonal structure with a unit cell defined by  $a = b = 4.366 \text{ \AA}$  and  $c = 4.953 \text{ \AA}$  according to the ICDS data files No. (00-006-0362). These results suggest that the phase AgTe transforms at 350 K to metastable phase and Se crystals. Further annealing temperature to 370 K the metastable AgTe phase and Se mixture transforms into stable AgTe and Se crystals with no glasses or crystalline metastable phase present.

## Conclusions

The kinetic mechanism of  $\text{Se}_{88}\text{Te}_{10}\text{Ag}_2$  glass has been studied using several theoretical methods under non-isothermal condition and conclusions gives as follows:

- The composition under study has single glass transition and two overlapping crystalline phases proved the homogeneity of the glass.
- The  $E_c$  valued deduced by Matusita et al. model shows strong heating rate dependence for the two phases.

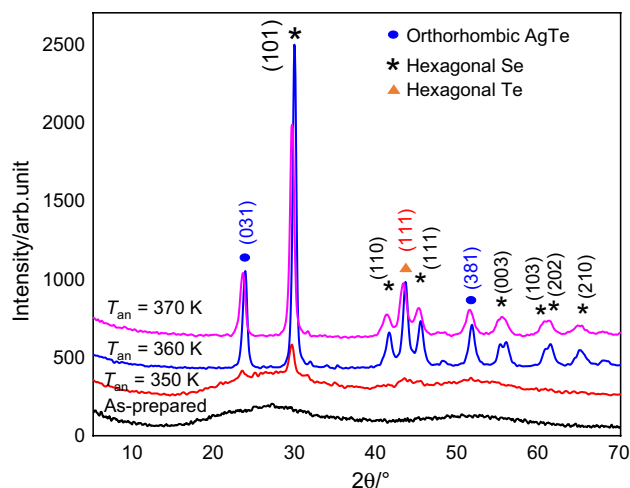


**Fig. 17** X-ray diffraction pattern of  $\text{Se}_{88}\text{Te}_{10}\text{Ag}_2$  glass for as prepared and annealed at different temperature for 1 h

- The average deduced  $n$  values by (JMA) model are not integers value this indicates the crystallization mechanism is composite.
- The experimental DSC scans are agreement with the JMA model only at low heating rates. While the Sestak–Berggren model  $\text{SB}(M, N)$  gives a better fitting to the measured DSC scans at all heating rates.
- The crystalline phases in DSC curves can be identified by X-ray diffraction (XRD) and SEM analysis.
- The dominate crystalline phases are Se and AgTe.

**Funding** Open access funding provided by The Science, Technology & Innovation Funding Authority (STDF) in cooperation with The Egyptian Knowledge Bank (EKB).

**Open Access** This article is licensed under a Creative Commons Attribution 4.0 International License, which permits use, sharing, adaptation, distribution and reproduction in any medium or format, as long as you give appropriate credit to the original author(s) and the source, provide a link to the Creative Commons licence, and indicate if changes were made. The images or other third party material in this article are included in the article's Creative Commons licence, unless indicated otherwise in a credit line to the material. If material is not included in the article's Creative Commons licence and your intended use is not permitted by statutory regulation or exceeds the permitted use, you will need to obtain permission directly from the copyright holder. To view a copy of this licence, visit <http://creativecommons.org/licenses/by/4.0/>.

## References

1. Atyia H, Fouad S, Sharma A, Mehta N. Linear and nonlinear optical properties of amorphous Se–Te–Sn–Cd films. *Phys B Condens*

- Matter. 2023;653:414672. <https://doi.org/10.1016/j.physb.2023.414672>.
2. Mahadevan S, Giridhar A, Singh A. Calorimetric measurements on as-sb-se glasses. *J Non-cryst Solids*. 1986;88(1):11–34. [https://doi.org/10.1016/S0022-3093\(86\)80084-9](https://doi.org/10.1016/S0022-3093(86)80084-9).
3. Chen R, Xu D, Guo G, Gui L. Preparation of  $\text{Ag}_2\text{Se}$  and  $\text{Ag}_2\text{Se}_{1-x}\text{Te}_x$  nanowires by electrodeposition from DMSO baths. *Electrochem Commun*. 2003;5(7):579–83. [https://doi.org/10.1016/S1388-2481\(03\)00133-4](https://doi.org/10.1016/S1388-2481(03)00133-4).
4. Mehta N, Kumar A. Comparative analysis of calorimetric studies in  $\text{Se}_{90}\text{M}_{10}$  ( $M = \text{In, Te, Sb}$ ) chalcogenide glasses. *J Therm Anal Calorim*. 2007;87(2):345–50. <https://doi.org/10.1007/s10973-005-7411-3>.
5. Abdel-Rahim M. A study of the crystallization kinetics of some Se–Te–Sb glasses. *J Non-cryst Solids*. 1998;241(2–3):121–7. [https://doi.org/10.1016/S0022-3093\(98\)00766-2](https://doi.org/10.1016/S0022-3093(98)00766-2).
6. Akiyama T, Uno M, Kitaura H, Narumi K, Kojima R, Nishiuuchi K, et al. Rewritable dual-layer phase-change optical disk utilizing a blue-violet laser. *Jpn J Appl Phys*. 2001;40(3S):1598. <https://doi.org/10.1143/JJAP.40.1598>.
7. Naqvi SF, Saxena N, Sharma K, Bhandari D. Glass-crystal transformations in  $\text{Se}_{80-x}\text{Te}_{20}\text{Ag}_x$  ( $x = 0, 3, 5, 7$  and  $9$ ) glasses. *J Alloys Compd*. 2010;506(2):956–62. <https://doi.org/10.1016/j.jallcom.2010.07.128>.
8. Mehta N, Kumar A. Observation of phase separation in some Se–Te–Ag chalcogenide glasses. *Mater Chem Phys*. 2006;96(1):73–8. <https://doi.org/10.1016/j.matchemphys.2005.06.044>.
9. Sharma D, Shukla R, Kumar A. Transient photoconductivity in amorphous thin films of  $\text{Se}_{75}\text{Te}_{20}\text{Ag}_5$ . *Thin Solid Films*. 1999;357(2):214–7. [https://doi.org/10.1016/S0040-6090\(99\)00648-3](https://doi.org/10.1016/S0040-6090(99)00648-3).
10. Mehta N, Zulfequar M, Kumar A. Crystallization kinetics of some Se–Te–Ag chalcogenide glasses. *J Optoelectron Adv Mater*. 2004;6:441–8.
11. Tiwari R, Kumar D, Mehta N. Amorphous to crystalline phase transition in glassy  $\text{Se}_{65}\text{Te}_{20}\text{Ag}_{15}$  alloy. *Phase Transit*. 2009;82(1):75–86. <https://doi.org/10.1080/01411590802361734>.
12. Wagner T. Photo- and thermally-induced diffusion and dissolution of Ag in chalcogenide glasses thin films. *J Optoelectron Adv Mater*. 2002;4(3):717–27.
13. Chou L-H, Chang Y-Y, Chai Y-C, Wang S-Y. Phases of the initial-ized AgInSbTe phase change optical recording films. *Jpn J Appl Phys*. 2001;40(8R):4924. <https://doi.org/10.1143/JJAP.40.4924>.
14. Šesták J, Berggren G. Study of the kinetics of the mechanism of solid-state reactions at increasing temperatures. *Thermochim Acta*. 1971;3(1):1–12. [https://doi.org/10.1016/0040-6031\(71\)85051-7](https://doi.org/10.1016/0040-6031(71)85051-7).
15. Banerjee S, Robi P, Srinivasan A. Calorimetric study of precipitation kinetics of Al–Cu–Mg and Al–Cu–Mg–0.06 wt.% Sn alloys. *Met Mater Int*. 2010;16:523–31. <https://doi.org/10.1007/s12540-010-0802-4>.
16. Málek J, Criado JM, Šesták J, Militký J. The boundary conditions for kinetic models. *Thermochim Acta*. 1989;153:429–32. [https://doi.org/10.1016/0040-6031\(89\)85452-8](https://doi.org/10.1016/0040-6031(89)85452-8).
17. Málek J. The applicability of Johnson–Mehl–Avrami model in the thermal analysis of the crystallization kinetics of glasses. *Thermochim Acta*. 1995;267:61–73. [https://doi.org/10.1016/0040-6031\(95\)02466-2](https://doi.org/10.1016/0040-6031(95)02466-2).
18. Málek J. Kinetic analysis of crystallization processes in amorphous materials. *Thermochim Acta*. 2000;355(1–2):239–53. [https://doi.org/10.1016/S0040-6031\(00\)00449-4](https://doi.org/10.1016/S0040-6031(00)00449-4).
19. Abdel-Rahim M, Hammam MA, Abu-Sehly A, Hafiz M. Composition effect on the pre-crystallization and crystallization characteristics for  $\text{Se}_{90-x}\text{Te}_{10}\text{Ag}_x$ . *J Alloys Compd*. 2017;728:1346–61. <https://doi.org/10.1016/j.jallcom.2017.09.004>.

20. Abdelazim N, Abdel-Latif A, Abu-Sehly A, Abdel-Rahim M. Determination of activation energy of amorphous to crystalline transformation for  $\text{Se}_{90}\text{Te}_{10}$  using isoconversional methods. *J Non-cryst Solids*. 2014;387:79–85. <https://doi.org/10.1016/j.jnoncrysol.2014.01.012>.
21. Lasocka M. The effect of scanning rate on glass transition temperature of splat-cooled  $\text{Te}_{85}\text{Ge}_{15}$ . *Mater Sci Eng*. 1976;23(2–3):173–7. [https://doi.org/10.1016/0025-5416\(76\)90189-0](https://doi.org/10.1016/0025-5416(76)90189-0).
22. Kissinger H. Variation of peak temperature with heating rate in differential thermal analysis. *J Res Natl Bur Stand*. 1956;57:217.
23. Hrubý A. Evaluation of glass-forming tendency by means of DTA. *Czechoslov J Phys B*. 1972;22(11):1187–93. <https://doi.org/10.1007/BF01690134>.
24. Matusita K, Komatsu T, Yokota R. Kinetics of non-isothermal crystallization process and activation energy for crystal growth in amorphous materials. *J Mater Sci*. 1984;19:291–6. <https://doi.org/10.1007/BF00553020>.
25. Lopes A, Monteiro R, Soares R, Lima M, Fernandes M. Crystallization kinetics of a barium–zinc borosilicate glass by a non-isothermal method. *J Alloys Compd*. 2014;591:268–74. <https://doi.org/10.1016/j.jallcom.2013.12.086>.
26. Majhi K, Varma K. Crystallization kinetic studies of  $\text{CaBi}_2\text{B}_2\text{O}_7$  glasses by non-isothermal methods. *J Mater Sci*. 2009;44:385–91. <https://doi.org/10.1007/s10853-008-3149-1>.
27. Liu F, Sommer F, Bos C, Mittemeijer E. Analysis of solid state phase transformation kinetics: models and recipes. *Int Mater Rev*. 2007;52(4):193–212. <https://doi.org/10.1179/174328007X160308>.
28. Kissinger HE. Reaction kinetics in differential thermal analysis. *Anal Chem*. 1957;29(11):1702–6. <https://doi.org/10.1021/ac60131a045>.
29. Lu W, Yan B, Huang W. Complex primary crystallization kinetics of amorphous Finemet alloy. *J Non-cryst Solids*. 2005;351(40–42):3320–4. <https://doi.org/10.1016/j.jnoncrysol.2005.08.018>.
30. Pustkova P, Švadlák D, Šhánělová J, Málek J. The non-isothermal crystallization kinetics of  $\text{Sb}_2\text{S}_3$  in the  $(\text{GeS}_2)_{0.2}(\text{Sb}_2\text{S}_3)_{0.8}$  glass. *Thermochim Acta*. 2006;445(2):116–20. <https://doi.org/10.1016/j.tca.2005.08.002>.
31. Wang J, Kou H, Li J, Gu X, Xing L, Zhou L. Determination of kinetic parameters during isochronal crystallization of  $\text{Ti}_{40}\text{Zr}_{25}\text{Ni}_8\text{Cu}_9\text{Be}_{18}$  metallic glass. *J Alloys Compd*. 2009;479(1–2):835–9. <https://doi.org/10.1016/j.jallcom.2009.01.072>.

**Publisher's Note** Springer Nature remains neutral with regard to jurisdictional claims in published maps and institutional affiliations.